ChemCatChem

Supporting Information

Ethylcyclohexane Hydroconversion in EU-1 Zeolite: DFT-based Microkinetic Modeling Reveals the Nature of the Kinetically Relevant Intermediates

Ester Gutierrez-Acebo, Jérôme Rey, Christophe Bouchy, Yves Schuurman,* and Céline Chizallet*

S1. Catalytic tests results

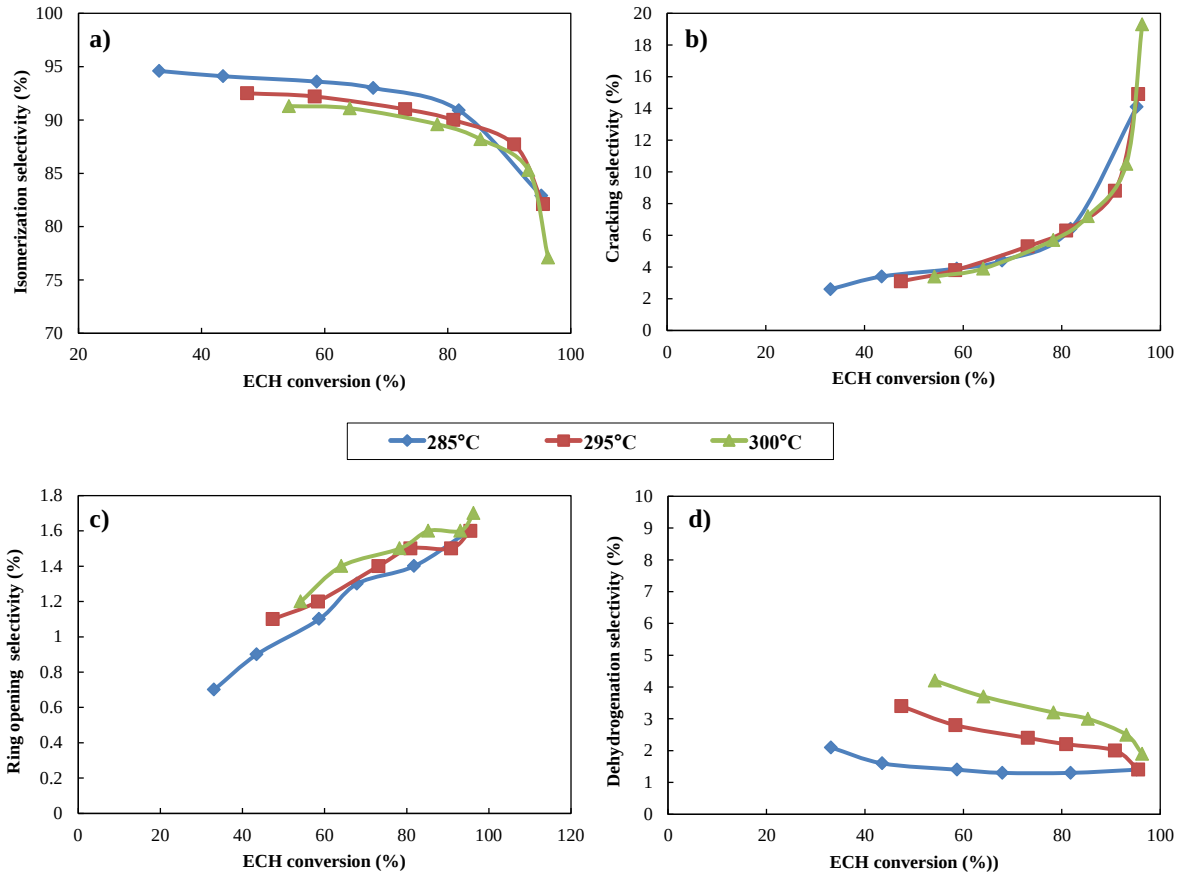

Figure S1. Evolution of the selectivity versus ECH conversion for the 1% Pt-Al_2O_3/H-EU-1 catalyst; a) isomerization; b) cracking; c) ring opening; d) dehydrogenation.

Figure S2 depicts the evolution of the mole percentage of all EMCP family isomers with ECH conversion. 13-EMCP appears as the major primary product of this family, regardless the position of the substituents (cis and trans i.e. C1E3MCP and T1E3MCP). Trans-1-ethyl,2-methyl-cyclopentane (T1E2MCP) appears in lower amount than 13-EMCP at low conversion. It increases as the conversion increases in detriment of 13-EMCP. The same tendency was observed concerning cis-1-ethyl-2-methyl-cyclopentane (C1E2MCP) and 1-ethyl,1-methyl-cyclopentane (1E1MCP). Nevertheless, their mole percentages remain lower and almost negligible compared to T1E2MCP and 13-EMCP (cis and trans) mole percentages. Only T1E3MCP and T1E2MCP mole percentages are slightly far from equilibrium for ECH conversion higher than 90%. As expected, the mole percentage of each molecule tends to approach the thermodynamic equilibrium value as the conversion increases.

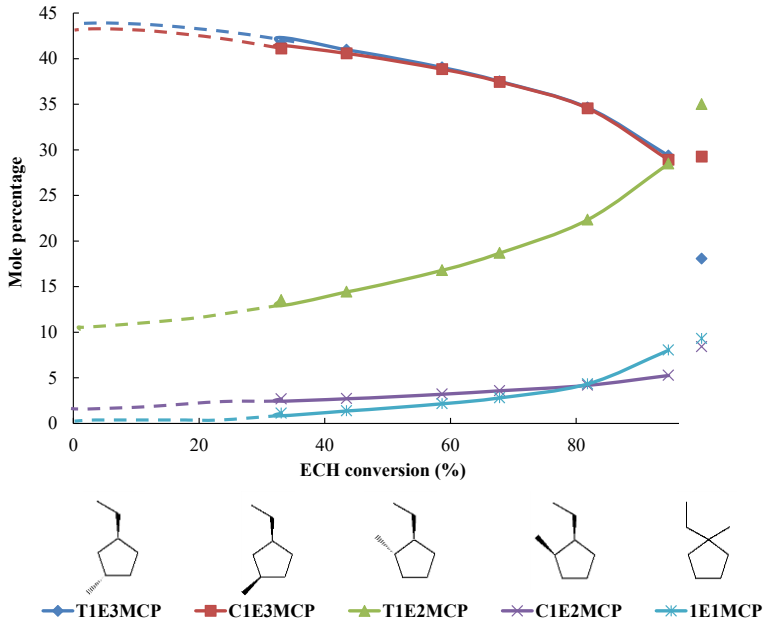

Figure S2. Isomers mole percentage within the EMCP family vs ECH conversion at 285°C in full lines. The free dots on the right correspond to the isomers mole percentage in equilibrium at 285°C according to PROII.

Figure S3 depicts the evolution of DMCH isomers with conversion. In this case, both, cis-1,3-dimethylcyclohexane (C13DMCH) and cis-1,4-dimethyl-cyclohexane (C14DMCH) are the primary products of the DMCH isomers family with a small fraction of trans-1,3-dimethylcyclohexane (T13DMCH) plus trans-1,4-dimethyl-cyclohexane (T14DMCH). Note that T13DMCH and T14DMCH cannot be separated as they are coeluted in gas chromatography. From thermodynamic calculations (as calculated with ProII), it was found that the ratio cis/trans 13-DMCH is equal to 2.9±0.1 in the temperature range of 280-300°C. This ratio was used to correct the 14-DMCH and 13-DMCH fractions in the model. The 14-DMCH fraction thus contains the trans-13-DMCH fraction. Nonetheless, C13DMCH is the major product at lower conversion. The mole percentage of T13DMCH plus T14DMCH increases with the ECH conversions in detriment of the C13DMCH, whereas the C14DMCH slightly decreases, and the trans-1,2-dimethyl-cyclohexane (T12DMCH) increased reaching its highest mole percentages (14%) at higher conversions. The amounts of cis-1,2-dimethyl-cyclohexane (C12DMCH) and 1,1-dimethyl-cyclohexane (11DMCH) remain lower on the whole ECH conversion range, reaching their higher mole percentage at higher conversions, 4 and 7% respectively.

With regards to the mole percentage at equilibrium in this group, half of the isomers are rather far from equilibrium even for a conversion higher than 90%. Only the isomers appearing experimentally at lower mole percentages such as C12DMCH, 11DMCH and T12DMCH get close to equilibrium. Regarding the major isomers T14DMCH plus T13DMCH and C14DMCH mole percentages are higher than their corresponding value at equilibrium. In the case of C13DMCH, the experimental mole percentage is far lower than the thermodynamic one. The main idea extracted from Figure 5.6 is that the mole percentages of C13DMCH and T14DMCH + T13DMCH are moving further from the thermodynamic equilibrium value as the conversion increases. At the moment we cannot provide satisfactory explanation for such phenomenon.

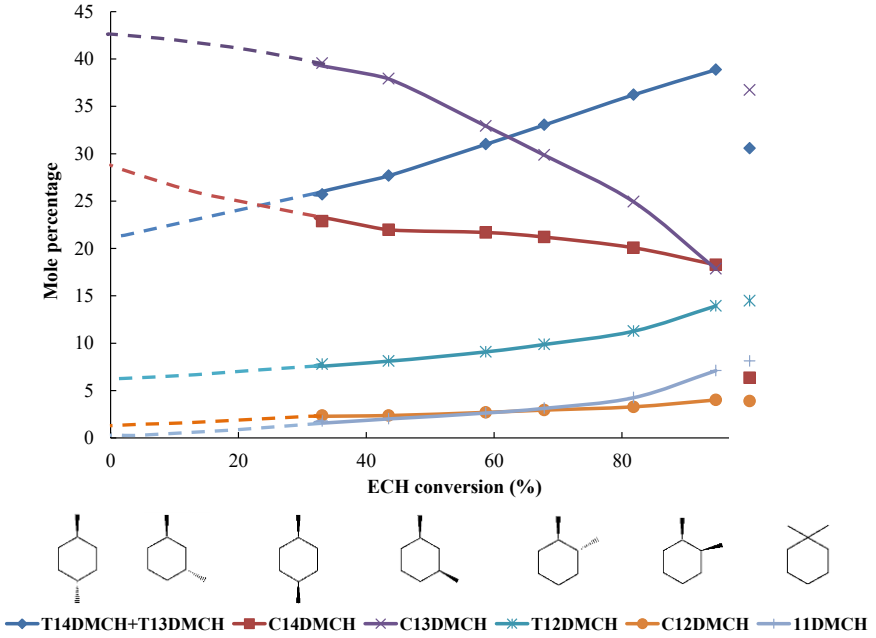

Figure S3. Isomers within the DMCH family mole percentage vs ECH conversion at 285°C in full lines. The free dots on the right correspond to the isomers mole percentage in equilibrium at 285°C according to PROII.

In the case of the TMCP isomers family (Figure S4), clearly trans-1,2-cis-2,4-trimethyl-cyclopentane (T12C24TMCP) is the major primary product appearing at low conversion. At the same time, it seems that cis-1,2-cis-2,4-trimethyl-cyclopentane (C12C24TMCP), trans-1,2-cis-2,3-trimethyl-cyclopentane (T12C23TMCP) and 1,1,3-trimethyl-cyclopentane (113TMCP) are primary products as well, but in lower amounts than T12C24TMCP. Besides, 1,1,2-trimethyl-cyclopentane (112-TMCP) is not a primary product in this family group. For conversions higher than 90%, the isomers with lower mole percentages are close to equilibrium, contrary to the isomers appearing in higher amounts. The same tendency was observed in the previous group (DMCH). In this case, T12C24TMCP experimental mole percentage is slightly higher than at equilibrium whereas T12C23TMCP mole percentage is lower than the equilibrium one. The most striking fact is that the experimental 113-TMCP mole percentage is much higher than the thermodynamic mole percentage. Thus, the production of this isomer seems favored by the intrinsic kinetics of the zeolite.

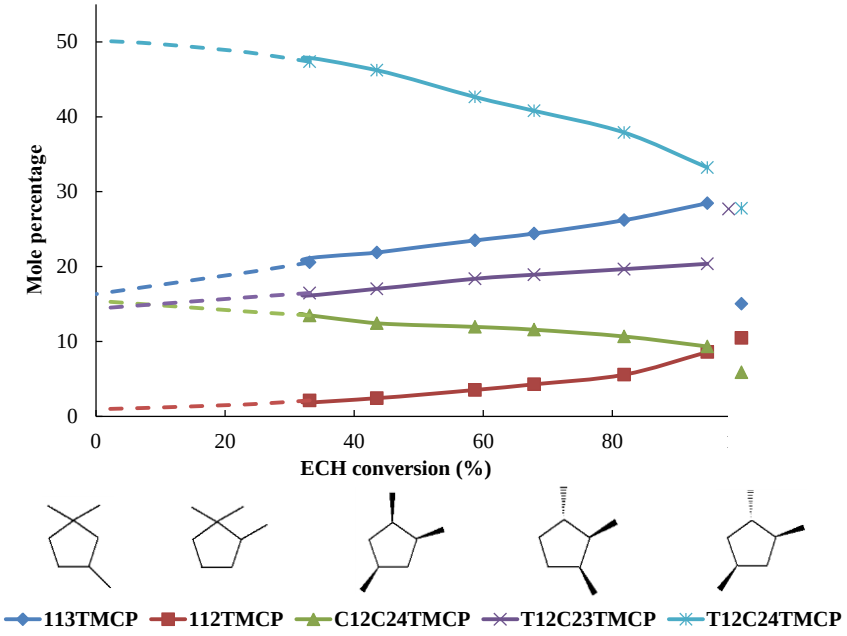

Figure S4. Isomers within the TMCP family mole percentage vs ECH conversion at 285°C in full lines. The free dots on the right correspond to the isomers mole percentage in equilibrium at 285°C according to PROII.

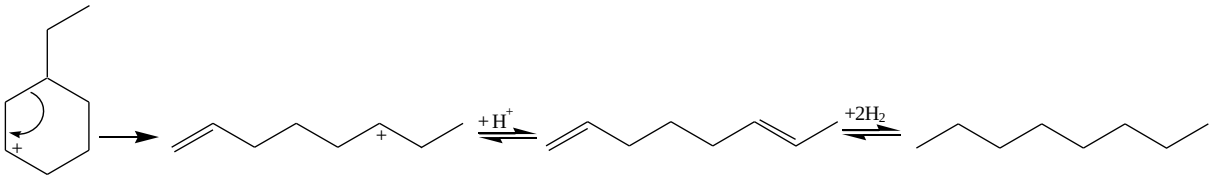

Figure S5. Possible ring opening pathway providing n-octane.

S2. *Ab initio* calculations and considered reaction steps

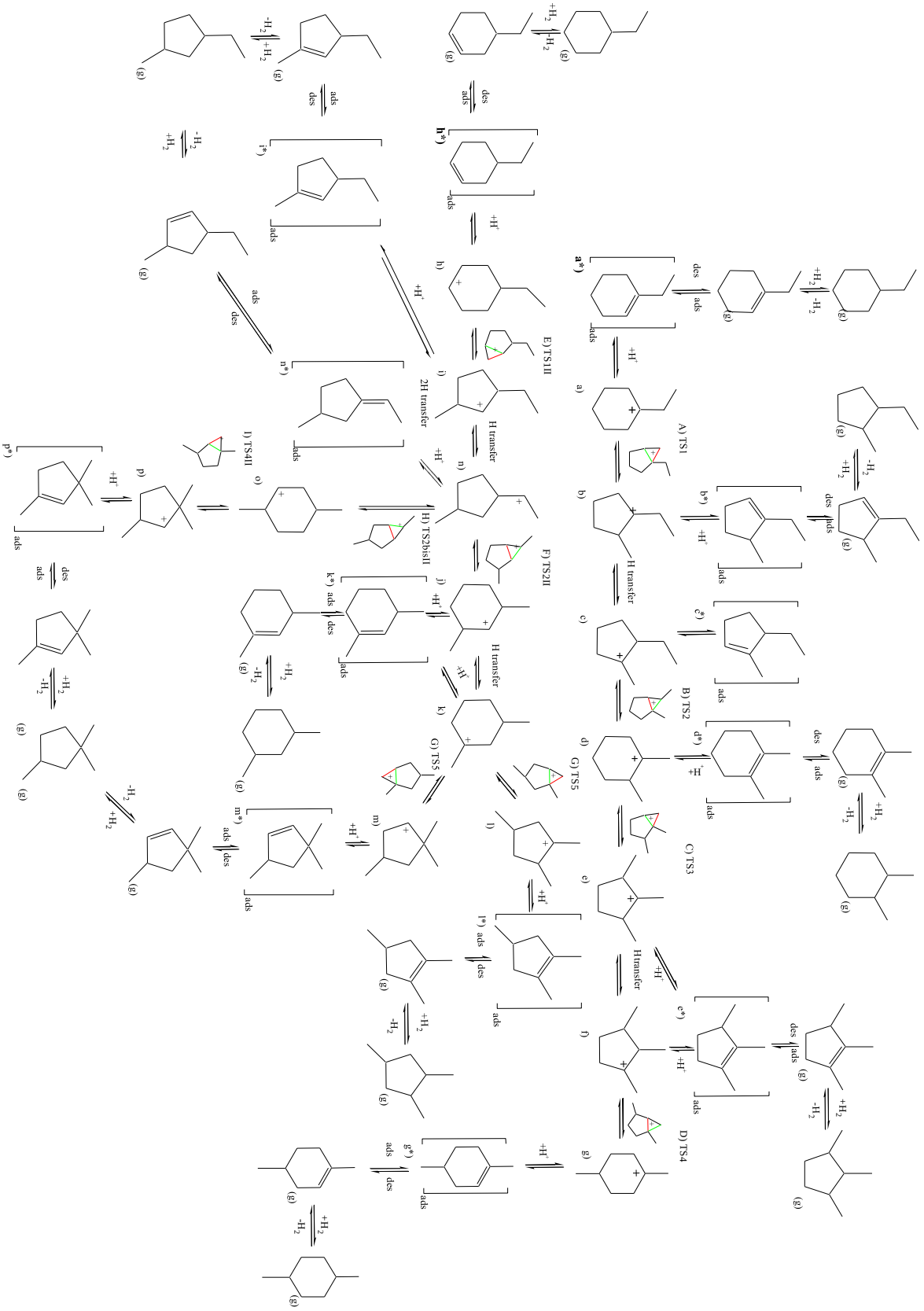

Figure S6. Reaction scheme considered in *ab initio* calculations and kinetic model for the hydroisomerization of ECH. Only isomers obtained through cycle contraction-expansion are shown, but methyl and hydride shifts were also considered in the micro-kinetic model.

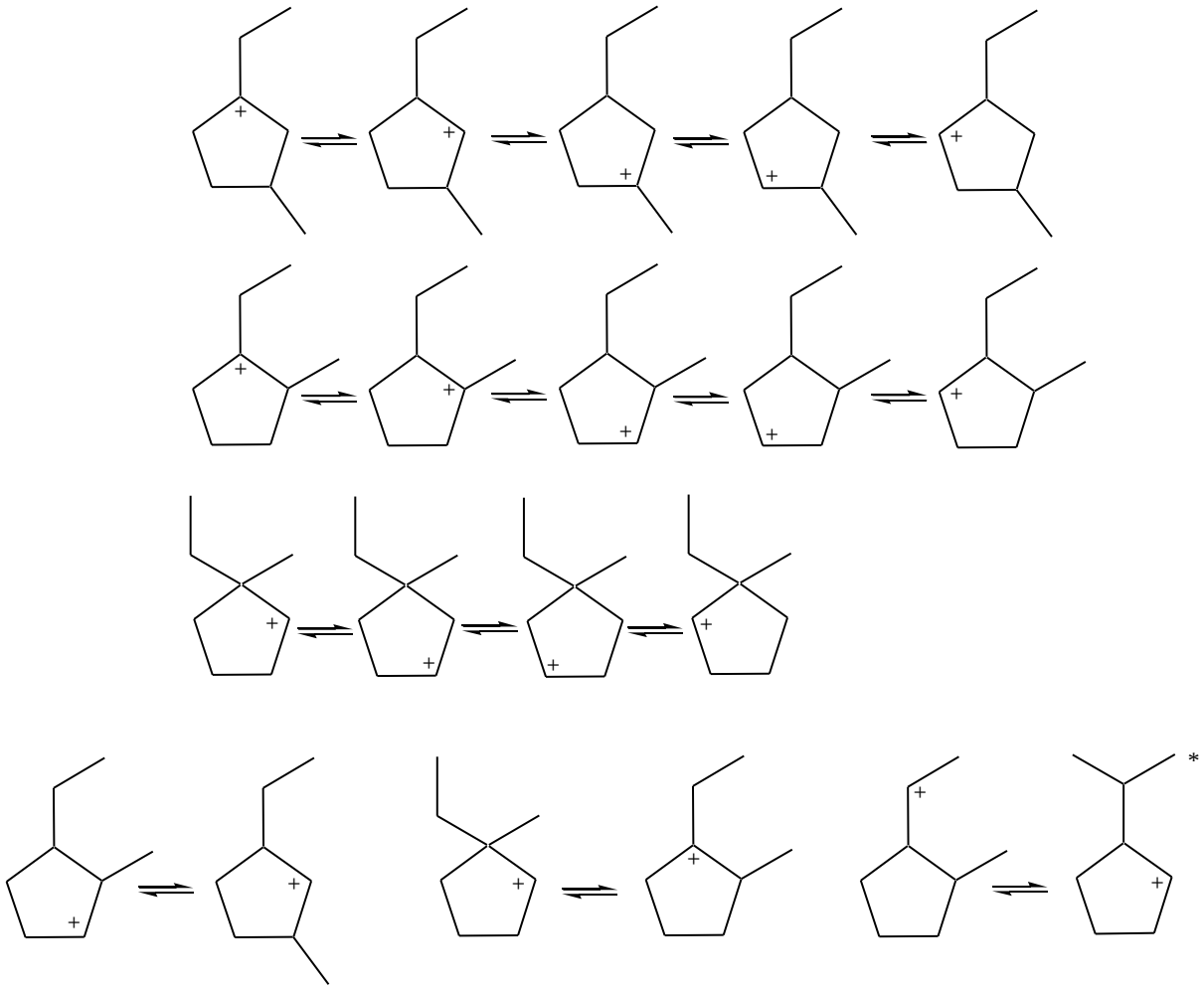

Figure S7. Hydride- and methyl-shifts within the EMCP family (*IPCP – isopropyl-cyclopentane).

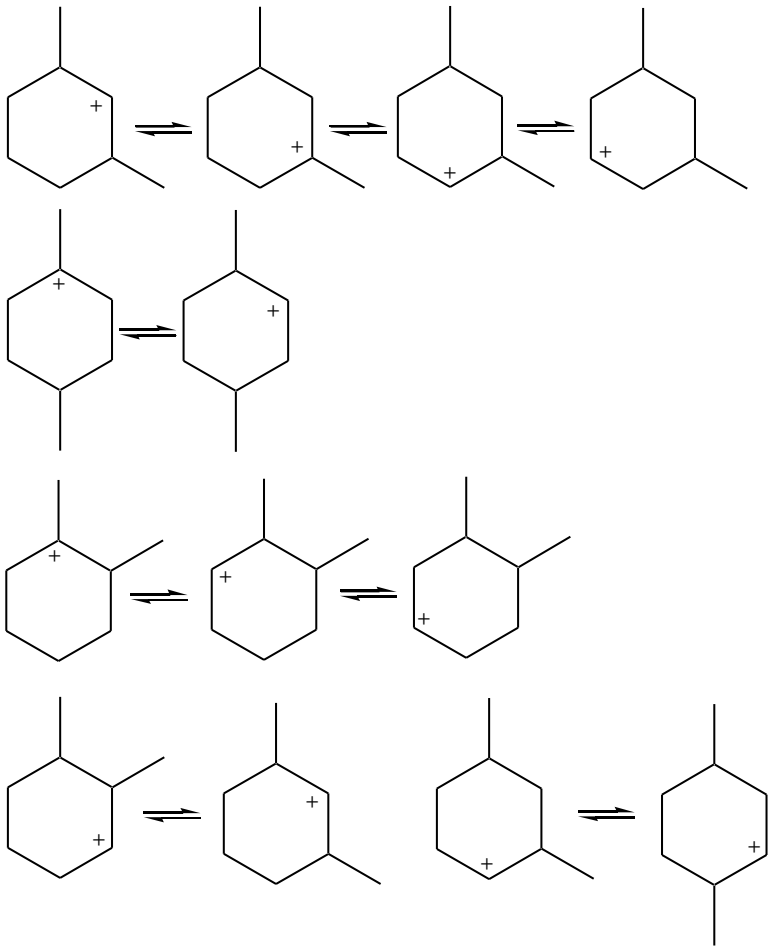

Figure S8. Hydride- and methyl-shifts within the DMCH family.

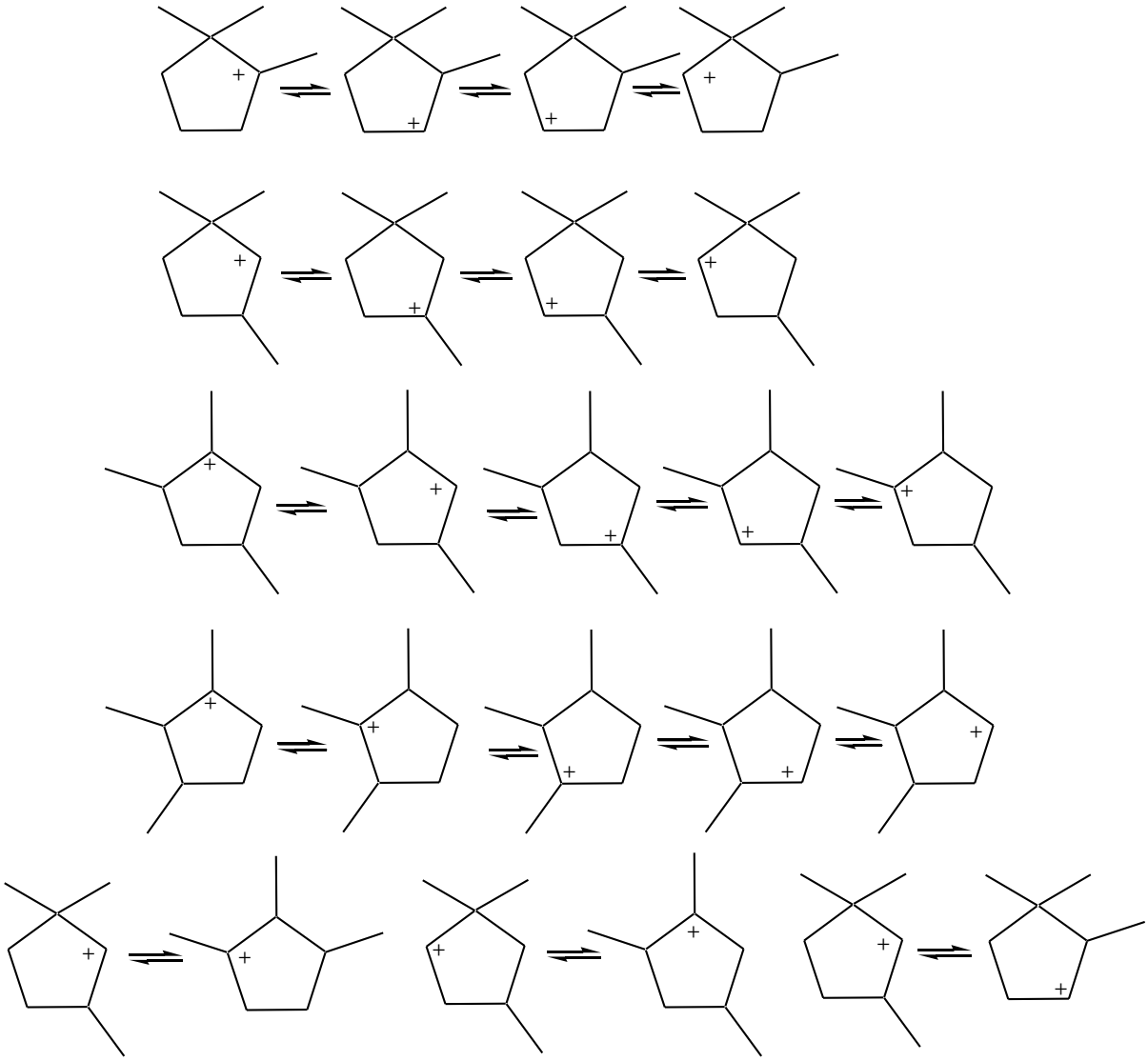

Figure S9. Hydride- and methyl-shifts within the TMCP family.

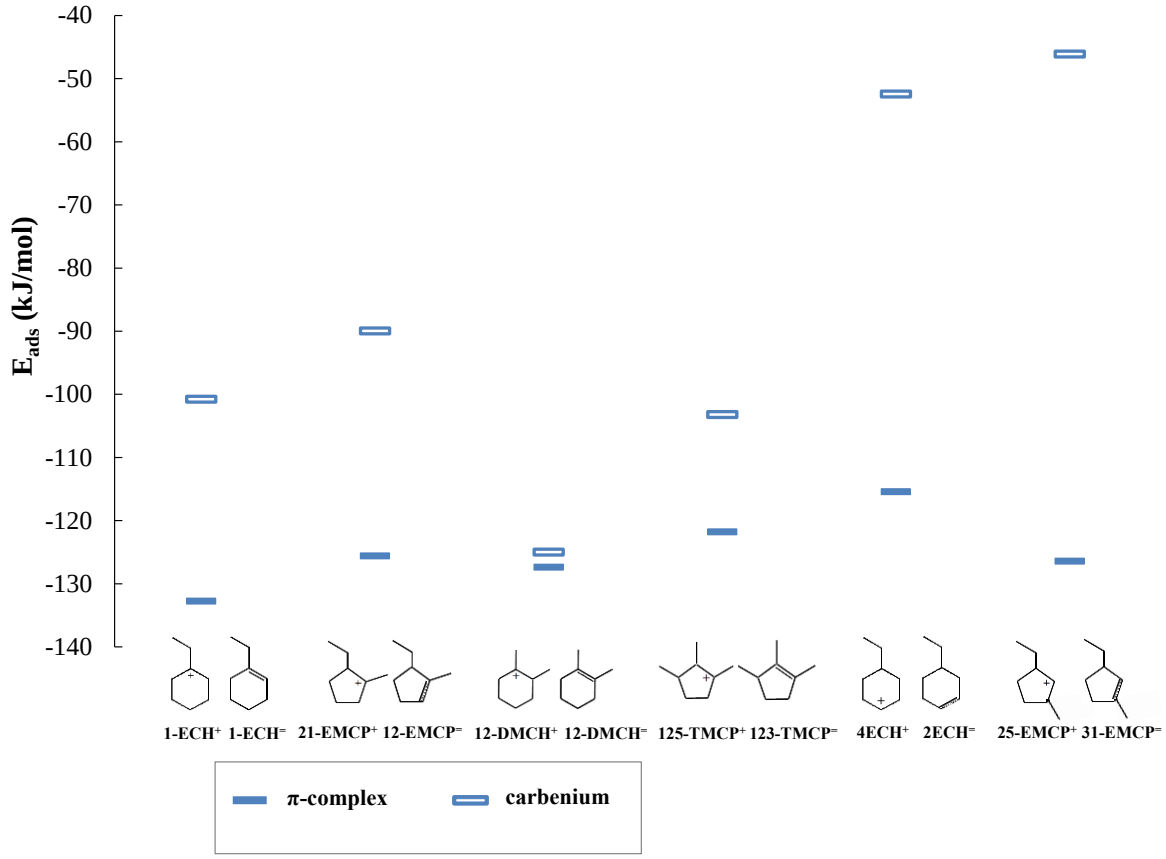

Figure S10. Adsorption energies for C8 π-complexes, tertiary and secondary carbenium ions at the T_1O_1 channel Brønsted site.

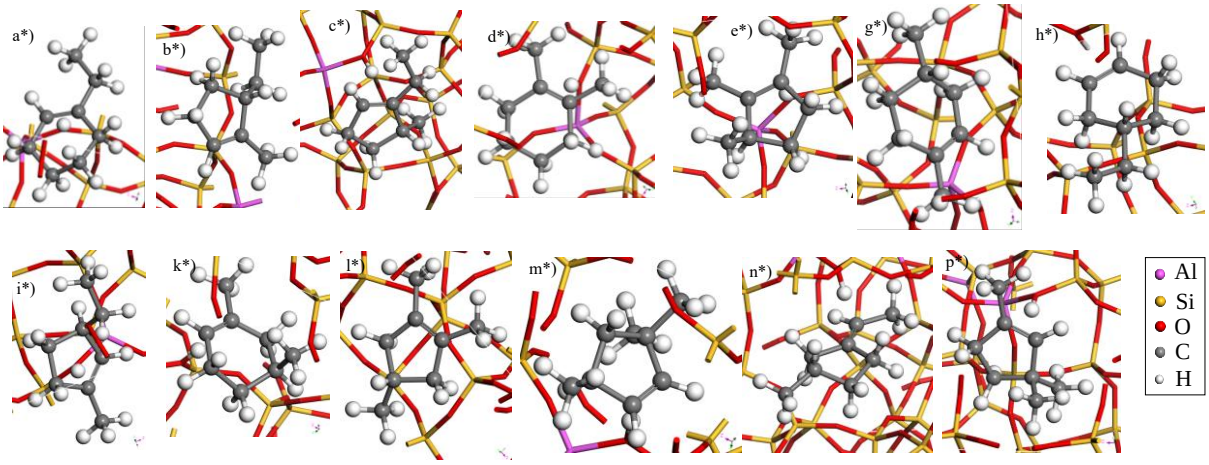

Figure S11. Structure of the calculated π-complexes at the T_1O_1 channel site.

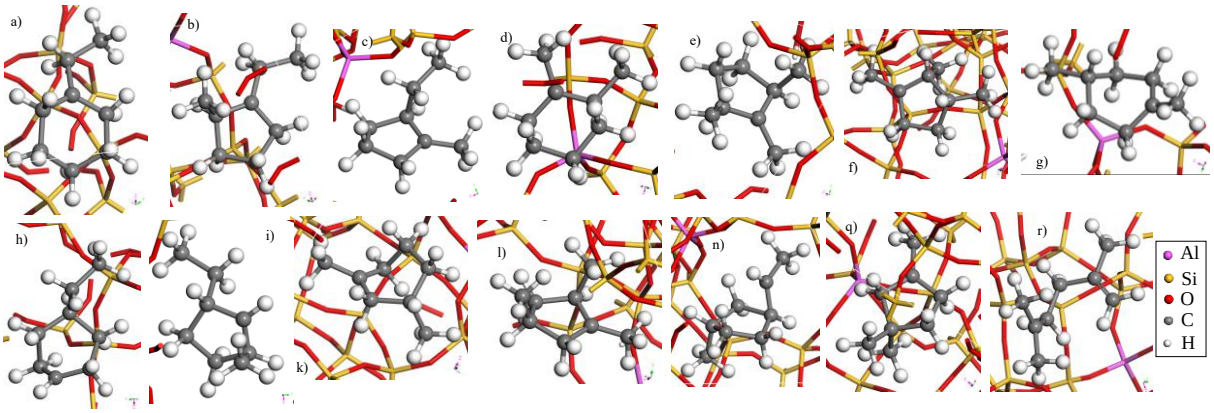

Figure S12. Structure of the calculated carbenium ions (local energy minima) at the T_1O_1 channel site.

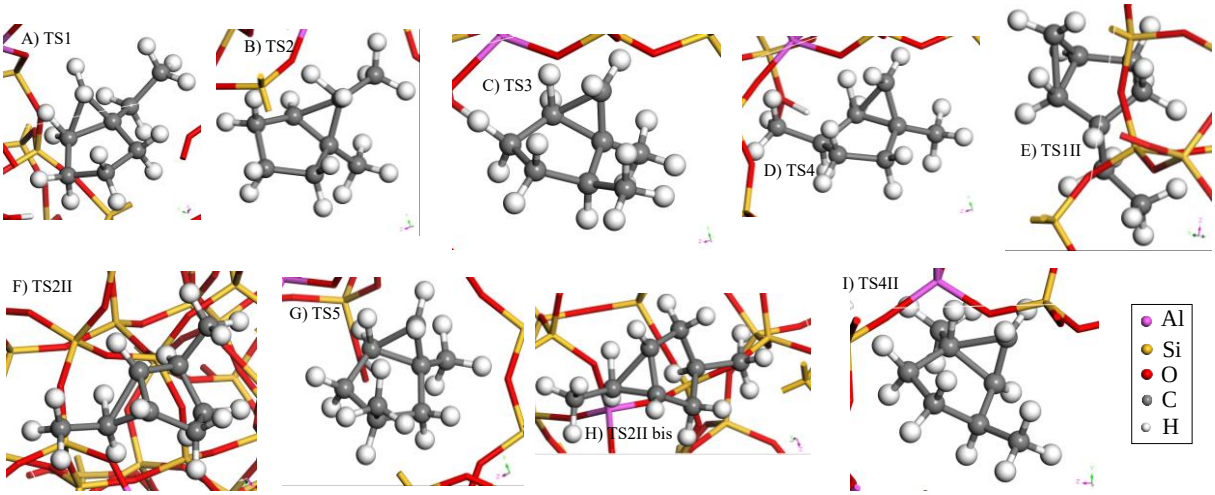

Figure S13. Structure of the calculated PCP transition states at the T_1O_1 channel site.

Table S1. Structural and frequency data for the transition states corresponding to Figure S13. C_2-C_3 holds the edge H, C_1-C_3 is the edge between the C3 and the C5 cycles, C_1-C_2 is the last edge of the triangle of the PCP. "H" corresponds to the edge-H of the PCP.

Species	C_1-C_2 (Å)	C_2-C_3 (Å)	C_3-C_1 (Å)	C_2-H (Å)	C_3-H (Å)	Imaginary frequency (cm^{-1})
A	1.472	1.709	1.546	1.428	1.261	413
B	1.576	1.734	1.462	1.209	1.576	196
C	1.463	1.709	1.558	1.468	1.239	292
D	1.488	1.747	1.530	1.358	1.267	322
E	1.466	1.771	1.548	1.440	1.208	384
F	1.533	1.808	1.476	1.214	1.455	432
G	1.459	1.713	1.569	1.484	1.226	326
H	1.533	1.806	1.477	1.213	1.456	428
I	1.432	1.760	1.609	1.620	1.183	127

Table S2. Energies, enthalpies, entropies and Gibbs free energies of all the relevant intermediates and transition states. All energies are referenced to the isolated 1-ethylcyclohexene molecule and the empty zeolite. Species that are involved in the definition of the elementary steps in the kinetic modeling are shown in bold.

		G_{ads} (kJ/mol)	H_{ads} (kJ/mol)	S_{ads} (J/K/mol)	E_{ads} (kJ/mol
	a*	**-28**	**-128**	**-182**	**-133**
	a	-17	-97	-146	-101
	A	**71**	**-46**	**-211**	**-43**
	b	**-34**	**-113**	**-143**	**-114**
	b*	16	-102	-216	-108
	c	6	-86	-167	-90
	c*	-26	-121	-173	-126
	B	**71**	**-38**	**-199**	**-37**
Path I	**d**	**-22**	**-120**	**-177**	**-125**
	d*	-9	-119	-201	-127
	C	**54**	**-55**	**-198**	**-52**
	e	-17	-100	-151	-103
	f	**-22**	**-94**	**-130**	**-96**
	e*=f*	-18	-117	-179	-122
	D	**60**	**-43**	**-187**	**-39**
	g	-5	-90	-153	-93
	g*	**-19**	**-110**	**-166**	**-116**
	h	51	-45	-174	-52
	h*	**-16**	**-126**	**-201**	**-113**
	E	**86**	**-27**	**-205**	**-27**
	i	65	-40	-191	-46
	i*	**-29**	**-122**	**-170**	**-126**
	n	-27	-68	-73	-86
Path II	n*	-21	-125	-189	-128
	F	**50**	**-51**	**-184**	**-50**
	k	18	-85	-187	-90
	k*	**-24**	**-109**	**-154**	**-116**
	G	**70**	**-45**	**-210**	**-43**
	l	2	-89	-166	-92
	l*	**-26**	**-134**	**-195**	**-137**
	m*	15	-84	-181	-90
	q	**-29**	**-126**	**-176**	**-125**
Path II bis	q*	-22	-129	-196	-133
	r	**38**	**-39**	**-140**	**-37**
	r*				**-52**
	H	**44**	**-49**	**-169**	**-47**
	o*=g*	**-19**	**-110**	**-166**	**-116**
Path II ter	**I**	**71**	**-42**	**-206**	**-42**
	p*=q*	-22	-129	-196	-133
	q	**-29**	**-126**	**-176**	**-125**

S3. Microkinetic modelling

The dehydrogenation/hydrogenation steps were assumed to be quasi-equilibrated and the concentration of gas phase olefins were calculated by:

$$P_{X^=} = \frac{P_X}{P_{H_2}} exp\left(\frac{\Delta S_{deh}}{R}\right) exp\left(\frac{-\Delta H_{deh}}{RT}\right) \quad \text{Eq. (S1)}$$

The adsorption/desorption of the olefins was calculated from the corresponding rate equation:

$$r_{ads/des} = k_{ads} P_{X^=} N_V - k_{des}[X^=_{ads}] \quad \text{Eq. (S2)}$$

The protonation/deprotonation steps were assumed to be quasi-equilibrated and the concentration of protonated surface species were calculated by:

$$[X^+_{ads}] = [X^=_{ads}] exp\left(\frac{\Delta S_{pr}}{R}\right) exp\left(\frac{-\Delta H_{pr}}{RT}\right) \quad \text{Eq. (S3)}$$

where P_X is the partial pressure of species X (bar), $P_{X^=}$ the partial pressure of species $X^=$, the respective olefin of X (bar), N_V the number of vacant sites (mol/kg), [$X_{ads}^=$] the concentration of adsorbed olefin X (mol/kg) and [X_{ads}^+] the concentration of adsorbed protonated species X (mol/kg). The number of active sites was set at 0.06 mol/kg (order of magnitude of one third of the total number of Brønsted acid sites in the zeolite, as we consider channel sites, excluding other locations of sites). The dehydrogenation/hydrogenation and protonation/deprotonation entropies and enthalpies in the above two equations were calculated by DFT and are reported in Table S3. Adsorption of ethylcyclohexene leads to two surface π-complexes. The concentration of 25-EMCP= was calculated from the concentration of 12-EMCP$^=$ using the Gibbs free energies given in Figure 5.

The adsorption/desorption entropies and enthalpies were also calculated by DFT, but in order to compensate for inaccuracies in the DFT calculations, the sorption entropies were estimated by regression analysis of the complete experimental data set, while the values of the sorption enthalpies were set to the DFT values. The desorption rate constant was fixed for 1-DMCH at a large value (~10^{16}-10^{18} s^{-1}) to allow quasi-equilibrated sorption and the value of the adsorption constant was adjusted. The estimated sorption entropies are reported in Table S3. DFT calculations are accurate to approximately 0.1 eV, which results in more than an order of magnitude in the value of the rate constant due to the exponential relation between the entropy or enthalpy and the rate constant. As the reaction network consists of a series of steps, the DFT inaccuracy will propagate and the final result can be several orders of magnitude off. The parity plot between DFT entropies and the entropies estimated by regression is shown in Figure S14.

Table S3. Thermodynamic constants for adsorption, dehydrogenation and protonation reactions. Adsorption entropies (in bold) were estimated by regression analysis. Other data come from the DFT calculations.

N°	Reaction	adsorption		dehydrogenation		protonation	
		ΔS (J/K/mol)	**ΔH (kJ/mol)**	**ΔS (J/K/mol)**	**ΔH (kJ/mol)**	**ΔS (J/K/mol)**	**ΔH (kJ/mol)**
1	$ECH_{(g)} \rightleftarrows ECH^=$	**-254**	128	138.1	-94.0	-	-
2	$13\text{-}EMCP_{(g)} \rightleftarrows 13\text{-}EMCP^=$	**-193**	122	140.0	-137.0	-	-
3	$12\text{-}EMCP_{(g)} + H^+ \rightleftarrows 12\text{-}EMCP^+$	**-224**	102	165.8	-131.2	73.0	-11.0
4	$11\text{-}EMCP_{(g)} \rightleftarrows 11\text{-}EMCP^=$	**-229**	112	140.0	-131.0	-	-
5	$14\text{-}DMCH_{(g)} \rightleftarrows 14\text{-}DMCH^=$	**-222**	110	143.4	-126.5	-	-
6	$13\text{-}DMCH_{(g)} \rightleftarrows 13\text{-}DMCH^=$	**-192**	109	140.1	-124.6	-	-
7	$12\text{-}DMCH_{(g)} + H^+ \rightleftarrows 12\text{-}DMCH^+$	**-271**	119	130.0	-90.3	24.0	-1.0
8	$11\text{-}DMCH_{(g)} \rightleftarrows 11\text{-}DMCH^=$	**-185**	113	140.0	-134.0	-	-
9	$113\text{-}TMCP_{(g)} + H^+ \rightleftarrows 113\text{-}TMCP^+$	**-293**	129	137.2	-112.9	20.0	3.0
10	$112\text{-}TMCP_{(g)} \rightleftarrows 112\text{-}TMCP^=$	**-264**	126	140.0	-125.0	-	-
11	$124\text{-}TMCP_{(g)} \rightleftarrows 124\text{-}TMCP^=$	**-286**	134	140.1	-95.9	-	-
12	$123\text{-}TMCP_{(g)} + H^+ \rightleftarrows 123\text{-}TMCP^+$	**-260**	117	140.0	-96.3	49.0	23.0
13	$IPCP_{(g)} \rightleftarrows IPCP^=$	**-209**	126	140.0	-125.0	-	-
14	$CRACK_{(g)} + H^+ \rightleftarrows CRACK^+$	**-223 ±**	100	140.0	-125.0	-	-

		250					

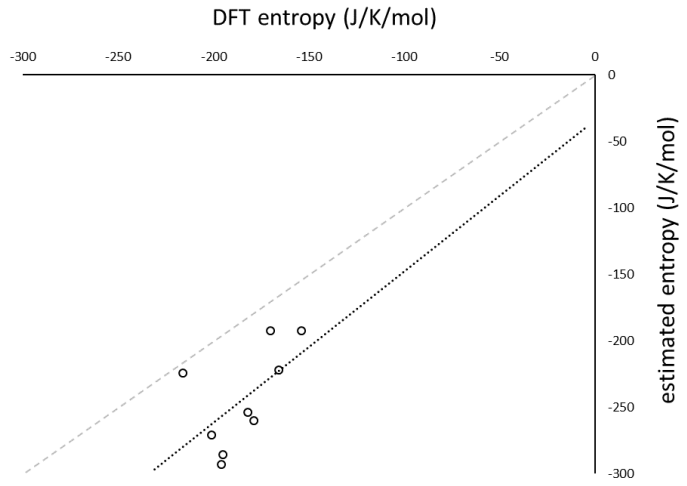

Figure S14. Parity plot for adsorption entropies, between DFT data and data obtained by regression.

The second section contains the isomerization and cracking steps of the surface intermediates. Reaction steps 15 – 25 (Table S4) corresponds to the *ab initio* calculations and the paths given in Scheme 4 and Figure 5. The corresponding values were fixed at their DFT values during parameter estimation. The formation of 11-DMCH and IPCP (Isopropyl-cyclopropane) were not included in the *ab initio* study. Therefore, the parameters for the pre-exponential factors of the forward reaction were estimated by regression analysis of the experimental data. Moreover, an additional cracking path was added from the 13-DMCH intermediate, to account for the different products inside the cracking fraction.

Table S4. Kinetic parameters for the isomerization, ring opening and cracking reactions. Parameters in bold are estimated by regression analysis. Other data come from the DFT calculations.

N°	Isomerization, ring opening or cracking	k^0_f (s^{-1})	k^0_b (s^{-1})	E_f (kJ mol^{-1})	E_b (kJ mol^{-1})
15	$ECH^{=} \rightleftarrows$ 12-$EMCP^{+}$	$3.33\ 10^{11}$	$3.13\ 10^{9}$	82.0	67.0
16	12-$EMCP^{+} \rightleftarrows$ 12-$DMCH^{+}$	$1.39\ 10^{10}$	$8.25\ 10^{11}$	75.0	82.0
17	12-$DMCH^{+} \rightleftarrows$ 123-$TMCP^{+}$	$9.46\ 10^{11}$	$3.34\ 10^{9}$	65.0	39.0
18	123-$TMCP^{+} \rightleftarrows$ 14-$DMCH^{=}$	$1.27\ 10^{10}$	$9.71\ 10^{11}$	51.0	68.0
19	$ECH_{=} \rightleftarrows$ 13-$EMCP^{=}$	$6.81\ 10^{12}$	$1.67\ 10^{11}$	100.0	95.0
20	13-$EMCP^{=} \rightleftarrows$ 13-$DMCH^{=}$	$2.22\ 10^{12}$	$3.48\ 10^{11}$	71.0	58.0
21	13-$DMCH^{=} \rightleftarrows$ 124-$TMCP^{=}$	$1.45\ 10^{10}$	$1.89\ 10^{12}$	64.0	88.0
22	13-$DMCH^{=} \rightleftarrows$ 113-$TMCP^{+}$	$1.45\ 10^{10}$	$1.94\ 10^{11}$	64.0	80.0
23	13-$EMCP^{=} \rightleftarrows$ 14-$DMCH^{=}$	$1.26\ 10^{13}$	$8.04\ 10^{12}$	73.0	62.0
24	14-$DMCH^{=} \rightleftarrows$ 113-$TMCP^{+}$	$9.67\ 10^{10}$	$3.17\ 10^{11}$	69.0	84.0
25	113-$TMCP^{+} \rightleftarrows$ $CRACK^{+}$	$8.24\ 10^{14}$	0	87.0	0
26	113-$TMCP^{+} \rightleftarrows$ 11-$DMCH^{=}$	$\mathbf{1.49 \pm 0.04\ 10^{13}}$	$4.68\ 10^{10}$	73.0	70.0
27	12-$EMCP^{+} \rightleftarrows$ $IPCP^{=}$	$\mathbf{4.44 \pm 0.01\ 10^{12}}$	$1.39\ 10^{10}$	88.0	77.0
28	13-$DMCH^{=} \rightleftarrows$ $CRACK^{+}$	$\mathbf{1.0 \pm 0.1\ 10^{10}}$	0	87.0	0

The third section contains the methyl-shifts that occur in the different reaction paths. DFT calculations showed that the enthalpies for these steps were small, typically less than 15 kJ/mol. They were set at 0 and the entropies were estimated by regression analysis (Table S5).

Table S5. Reaction entropies fitted by regression analysis for methylshifts. Reaction enthalpies were set at 0 in the microkinetic model.

N°	Methyl-shifts	ΔS (J/mol/K)
29	113-TMCP$^+$ ⇄ 112-TMCP$^=$	**-5**
30	113-TMCP$^+$ ⇄ 124-TMCP$^=$	**42**
31	12-DMCH$^=$ ⇄ 13-DMCH$^=$	**-22**
32	13-DMCH$^=$ ⇄ 14-DMCH$^=$	**-4**
33	12-EMCP$^+$ ⇄ 11-EMCP$^=$	**36**
34	12-EMCP$^+$ ⇄ 13-EMCP$^=$	**30**
35	113-TMCP$^+$ ⇄ 123-TMCP$^+$	**12**

The reactor is assumed to be an isothermal plug-flow pseudo-homogeneous packed bed reactor, without any heat and mass transfer limitations. It is modeled by the following differential equations for each component:

$$\frac{dF_i}{dW} = N_s \ \sum_j \upsilon_{ij}\, k_j P_{gas,i} \prod_{j'} \theta^m \qquad (mol/kg_{cat}/s) \qquad \text{Eq. (S4)}$$

where F_i is the molar flow rate of component i (mol/s), W is the catalyst mass (kg), Ns the concentration of active sites (mol/kg), k_j is the rate constant of the elementary step j, ν_{ij} the stoichiometric coefficient, $P_{gas,i}$ is the partial pressure of component i in the gas phase (bar), Θ is the fractional surface coverage of the surface intermediate, n, m are reaction orders that correspond to the stoichiometry of the elementary step (mass action law). In a microkinetic model the pseudo-steady state approximation is applied to the surface intermediates, setting their net production rate equal to zero. A site balance equation completes the set of equations that are solved numerically.

Analysis of all the 14-DMCH and 13-DMCH isomers was not possible (see Supporting Information S1). Co-elution of trans-13-DMCH with 14-DMCH isomers occurred. From thermodynamic calculations it was found that the ratio cis/trans 13-DMCH is equal to 2.9±0.1 in the temperature range of 280-300°C. This ratio was used to correct the 14-DMCH and 13-DMCH fractions in the model. The 14-DMCH fraction thus contains the trans-13-DMCH fraction.

The results obtained at 285°C, 295°C and 300°C are reported in Figure S15.

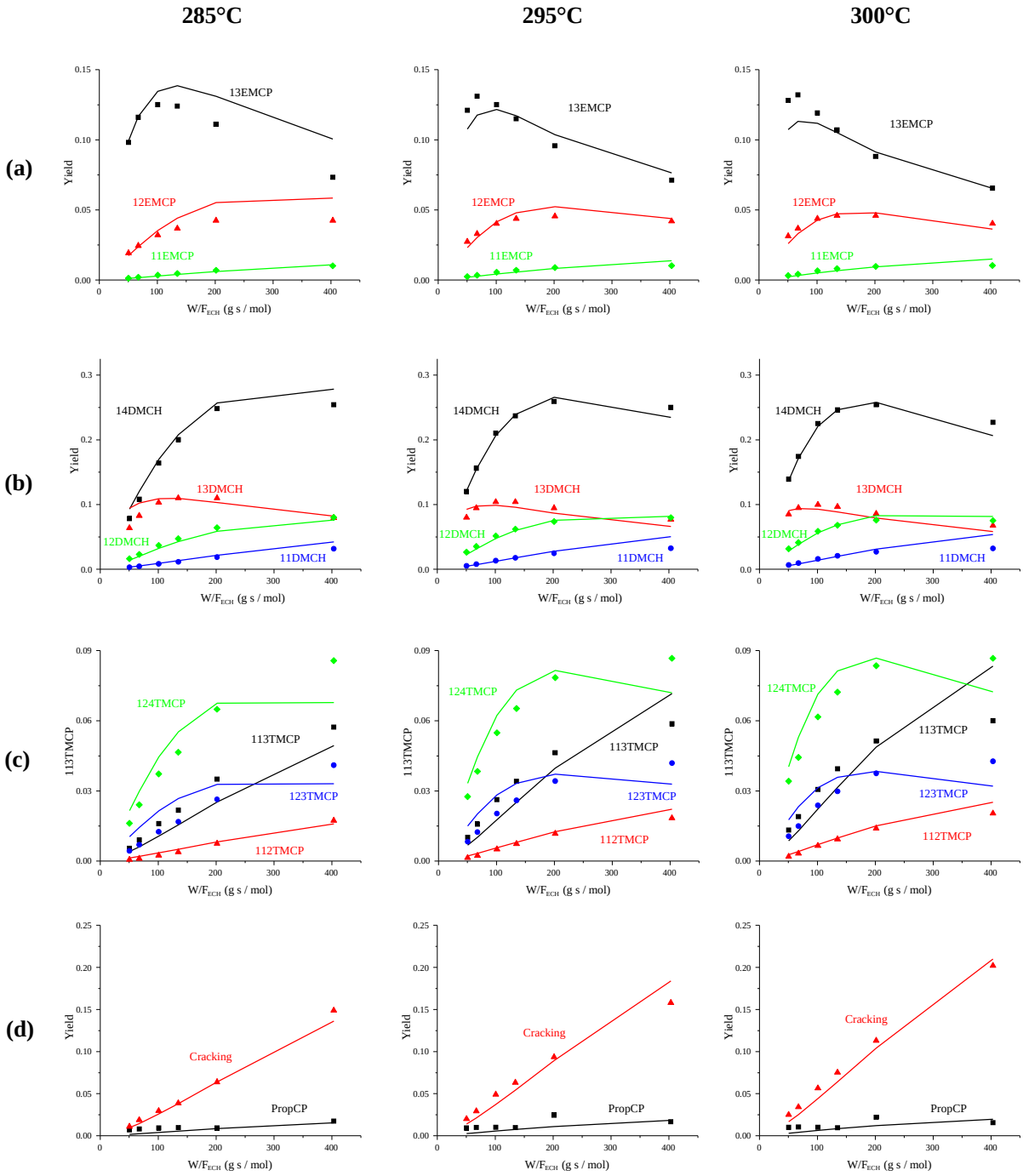

Figure S15. Yield in the different reaction products obtained experimentally (dots) and from DFT-based microkinetic modeling (lines) at 285°C (left), 295°C (center), 300°C (right). (a) EMCP, (b) DMCH, (c) TMCP, (d) PropCP and cracking products.